

Comparison of Analytical and Numerical Methods for PMSG Design Applied to D-Type Wind Generators

G. R. Bruzinga , A. J. Sguarezi Filho  Senior Member, IEEE, A. Pelizari  and I. Oliani 

Abstract—The objective of this work is to perform a comparative study between analytical and numerical methods (implemented via 2-D and 3-D FEM software) in 3.88 MVA, 710 V, 145 Hz permanent magnet synchronous generator (PMSG) design with a focus on wind power generation, for D-Type wind turbines. For this purpose an analytical solving method is proposed using NdFeB surface permanent magnet rotor. After this step the analytical results were compared with the numerical results and showed results with average relative error margin of about 3% (2-D simulation) and average absolute error of 37.3 mT (3-D simulation). In the second part of the design, AlNiCo PM were used in the rotor, however, the analytical and numerical results showed high average error, making the previous method, used for NdFeB PM, not suitable, requiring changes in the method. It is proposed then, a readjustment of the PM volume calculation, through analytical and numerical methodology. For the development of the method the main contributions were the modification of the table of speeds and frequencies from 60 Hz to 145 Hz, the creation of an extension parameter for the tip of the stator tooth to refine the airgap flux density calculation and the analytical solution of the rotor design when using AlNiCo PM. After these changes, the results obtained with a calculated average error margin of about 4% were satisfactory. The analytical and numerical results were commented and presented at the end of this work for the validation of the methodologies for both of PM (NdFeB and AlNiCo).

Index Terms—Finite Element Analysis, PMSG, Wind Generators

I. INTRODUCTION

D-Type wind turbines are topologies widely employed today. This type of wind turbine configuration uses, for interconnection to the grid, full capacity converters directly connected to its stator, as illustrated in Fig. 1 [1].

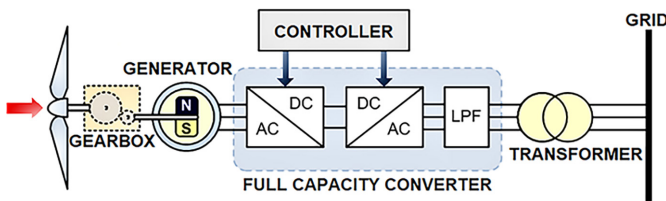


Fig. 1. D Type Wind Turbine.

For operation in D-Type topology, permanent magnet synchronous generators (PMSG) have excellent reliability, have

G. R. Bruzinga, A. J. Sguarezi Filho, A. Pelizari and I. Oliani are with the Universidade Federal do ABC - UFABC, Brazil. e-mails: gabriel.bruzinga@ufabc.edu.br, alfeu.sguarezi@ufabc.edu.br, ademir.pelizari@ufabc.edu.br and igor.oliani@ufabc.edu.br

low, medium, and high power applications, and can be used in vehicle traction systems as well as in wind turbines. PMSG have some advantages over conventional synchronous machines, such as high torque density and power density, simplified construction and maintenance of the machine, due to the absence of the DC excitation field winding, reducing losses and consequently obtaining higher efficiency, reducing maintenance, increasing its operation reliability [2], [3].

A. Motivation

The sizing of a PMSG requires some factors, including the operating power range, the types of permanent magnets (PM) used in the construction and their dimensions, the grid electrical frequency, stator sizing, rotor sizing, as well as the type of simulation employed, which can be 2-D or 3-D. Table I summarizes the main approaches used for PMSG design.

TABLE I
DESIGN METHODOLOGIES REFERENCES

Ref.:	Stator Design	PM Rotor	Frequency $f > 60$ Hz	Small PMSG	Large PMSG	Sizing Method	AlNiCo PM	NdFeB PM	2-D FEM	3-D FEM
[3]	no	no	yes	yes	no	no	no	yes	yes	no
[4]	yes	no	no	yes	yes	yes	no	no	no	no
[5]	no	yes	yes	yes	no	yes	no	yes	yes	no
[6]	no	yes	no	yes	no	no	no	yes	no	no
[7]	no	yes	yes	yes	no	no	no	yes	no	no
[8]	no	no	no	yes	no	no	no	no	yes	no
[9]	yes	no	no	yes	no	no	no	yes	no	no
[10]	no	no	yes	yes	no	no	no	yes	yes	no
[11]	no	no	yes	yes	no	no	yes	no	yes	no
[12]	no	no	no	yes	no	no	no	no	no	no
[13]	no	no	no	yes	no	no	no	yes	yes	no
[14]	no	no	no	yes	no	no	no	no	no	yes
[15]	no	no	no	yes	no	no	no	no	yes	no
[16]	yes	no	no	yes	no	yes	yes	no	yes	no

The main motivation of this work proposes a methodology that can be employed in the design of PMSG using two different types of PM for a frequency of 145 Hz with a focus on machines in the MW range.

The methodology applied in this work employs an approach not used in the references presented in Table I, including the design of the high power stator and rotor, the use of two different materials for the PM, one being more expensive (NdFeB) and an option with cheaper PM (AlNiCo) per kW, as well as 2-D and 3-D simulations [16].

However, the design of PMSG faces major challenges, among which are the complexity on design of PM magnetic circuit [17], [18], the best rotor topology [12], risk of demagnetization depending on the rotor magnets arrangement [11], and complicated estimation of air gap inductions [7], [15].

Thus, the use of analytical methods together with numerical methods present in finite element method (FEM) resolution software, for example, make the project, not less laborious, but more reliable, since it allows values obtained in both methods to be confronted [8], [9]. Such simulations allow the variation of several rotor PM arrangements, supporting the design and construction of an equipment of this complexity [5], [19]. The analytical method employed in this work are separated into two parts, the first of which focused on the development of the stator based on rated data, while the second part was intended for the sizing of the rotor [4], [20].

II. ANALYTICAL METHOD

In the rotor development stage, two PM with different materials were considered, being used sintered N-50 NdFeB and 72-LNGT Alnico PM, whose demagnetization curves are illustrated in Fig. 2.

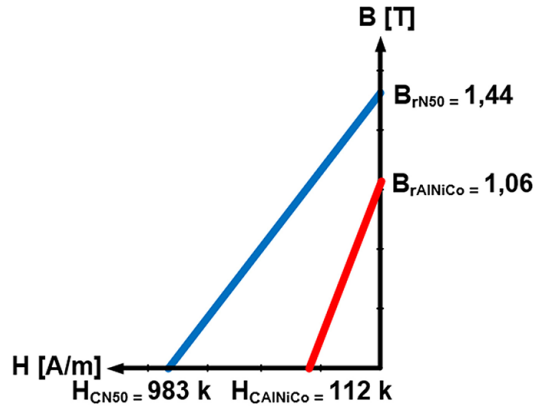


Fig. 2. PM Demagnetization Curve.

Fig. 3 presents the flowchart of the analytical solving illustrating all steps of the calculations, with due considerations and constraints of the design parameters.

A. Main Stator Dimensions

As a starting point for the stator design, the rated data of the machine was used, as shown in Table II [21].

TABLE II
RATED DATA

Parameter	Rated Value
Apparent Power (S_{VA})	3880000 VA
Active Power (P)	3298000 W
Line Voltage (V_l)	710 V
Electrical Frequency (f)	145 Hz
Synchronous Speed (n)	1450 rpm
Number of Phases (N_{phase})	3
Efficiency (η)	85%

Based on the electrical frequency and the rated speed, the number of pole pairs is determined as follows in (1).

$$p = \frac{60 \cdot f}{n} \quad (1)$$

Then the number of slots per pole and phase N_{CPF} and the shape factor K_f (pure sinusoidal wave: 1.11) is adopted. The

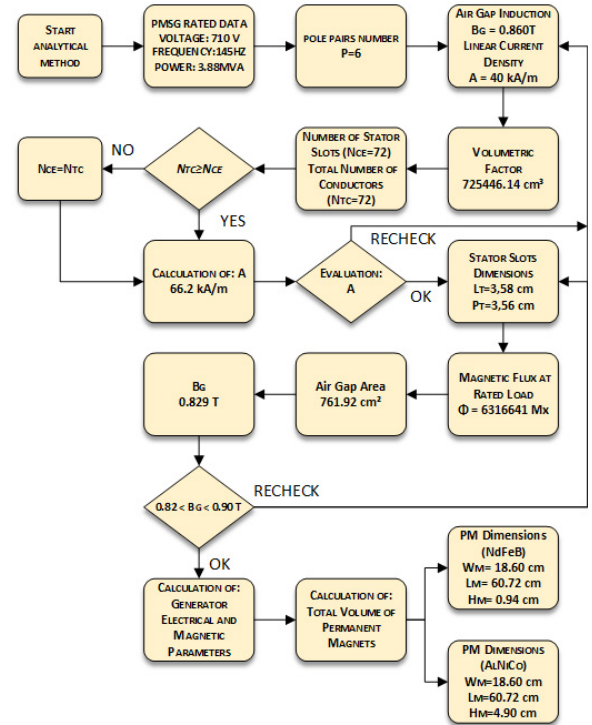


Fig. 3. Analytical Solving Flowchart.

number of slots per pole and phase is directly related to the winding factor of the three-phase synchronous machine K_a . In Table III the winding factor is determined as a function of the number of slots per pole [4].

TABLE III
WINDING FACTOR

N_{CPF}	K_a
1	1.000
2	0.966
3	0.960
4	0.958
5	0.957
6	0.956

Once the number of slots per pole and phase is defined, the number of poles and the number of phases, the total number of stator slots is determined as (2) [4].

$$N_{CE} = N_{CPF} \cdot 2p \cdot N_{phase} \quad (2)$$

The air gap flux density B_g , as well as the linear current density A (electric loading index), can be determined as a function of the number of poles, according to Table IV, which presents suggested ranges [4].

Based on the number of poles, the winding form factor, the air gap flux density and the linear current density, the volumetric factor is determined, which relates the diameter and the generator magnetic length:

$$M = \frac{S_{VA} \cdot 10^5}{K_a \cdot K_f \cdot n \cdot B_g \cdot A} = D_{int}^2 \cdot L_{mag} \quad (3)$$

TABLE IV
PRE-DETERMINED B_g AND A

Number of Poles	B_g (T)	A (A/m)
2	0.610 - 0.720	22000 - 65000
4	0.710 - 0.745	26000 - 40000
6	0.760 - 0.810	25000 - 45000
8	0.820 - 0.875	31000 - 50000
12	0.820 - 0.900	26000 - 54000

In (3) the units are expressed according to the international system (SI). The unit VA being expressed as $Kg.m^2/s^3$, the unit T being expressed as $Kg/A.s^2$ and considering n being expressed in Hz and subsequently as s^{-1} . Dimensional analysis was performed, resulting in:

$$M = \frac{[kg.m^2.s^{-3}]}{[s^{-1}].[kg.A^{-1}.s^{-2}].[A.m^{-1}]} = [m^3]$$

In (3) L_{mag} is the generator magnetic length and D_{int} is the stator inner diameter. The generator geometric length L_{geo} is determined based on the magnetic length with two ventilation slots and an additional length over the magnetic length due to ferromagnetic material lamination.

The stator inner diameter is determined by (4).

$$D_{int} = \sqrt[3]{\varepsilon \cdot M} \quad (4)$$

Where ε is defined as the ratio between the stator inner diameter and the magnetic length.

1) *First modification*: In the [4] method, the values of ε were determined as a function of the number of poles, specifically for a frequency of 60 Hz. For PMSG studied with nominal frequency of 145 Hz the values of ε were recalculated by linear interpolation. The Table V presents the recalculated ε values.

TABLE V
FREQUENCY AND ε RATIO

p	n (60Hz)	$\varepsilon(60Hz)$	n (145Hz)	$\varepsilon(145Hz)$
1	3600	1.3	8700	1.0
2	1800	1.6	4350	1.2
4	900	2.1	2175	1.5
6	600	2.7	1450	1.8

2) *Second modification*: The main stator dimensions are considered for the calculation of the respective areas. A parameter has been added to adjust the width of the stator teeth tips. It is observed in Fig.4 the variable μ_D that represents this increase (in cm). The purpose of this adjustment is to achieve the desired air gap flux density value [13].

The stator pole pitch τ was defined as the ratio between the stator inner circumference and the number of poles, while the stator teeth pitch τ_c was determined ratio between the inner

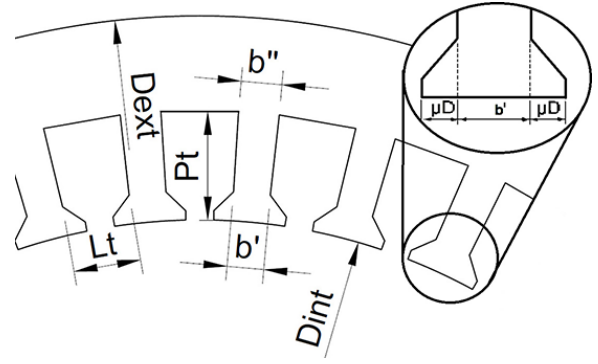


Fig. 4. Main Stator Parameters.

circumference of the stator and the number of stator slots. The rotor pole pitch b_p was fixed at 65% of the stator pole pitch length τ , avoiding the magnetic short circuit between the PM, and can be calculated by [4], [19]:

$$\psi = \frac{b_p}{\tau} \quad (5)$$

The number of stator conductors N_{TC} depends on the linear current density, the stator inner diameter and phase current, and can be determined by (6).

$$N_{TC} = \frac{A \cdot \pi \cdot D_{int}}{10^2 \cdot I_p} \quad (6)$$

The generator conductors are formed by a set of cables C_c , with section S_c and diameter D_C , to ensure a maximum current density σ [4]. Thus, the number of cables required to compose the generator conductors, becomes:

$$C_c = \frac{I_p}{\sigma \cdot S_c} \quad (7)$$

Once the number of cables is determined, the stator slots dimensions are calculated, considering the necessary insulations and spacings. Taking the width, C_L cables were used, the required insulation and spacings R_L , resulting in the total slot width L_t . The total slot depth P_t , was determined in a similar manner, considering C_P cables at the depth, so that $C_c = C_L \cdot C_P$ and their respective insulation and spacings R_P [4].

Once L_t and P_t have been calculated the stator tooth openings at the top (b') and at the stator wheel (b'') are determined. The tooth apertures become:

$$b' = \tau_c - L_t \quad (8)$$

And in turn, the opening of the tooth on the stator wheel is

$$b'' = \frac{b' \cdot (D_{int} + P_t)}{D_{int}} \quad (9)$$

With the main geometrical, electrical, and magnetic parameters calculated, the magnetic flux (ϕ) under rated load conditions is determined:

$$\phi = \frac{1,15 \cdot \sqrt{3} \cdot 10^8 \cdot V_l}{6 \cdot K_a \cdot K_f \cdot f \cdot N_{CF}} \quad (10)$$

To calculate the stator outer diameter (D_{ext}) it was necessary to predefine stator yoke flux density (B_{rce}) [4], which enabled the stator area (S_{CE}) to be determined:

$$S_{ce} = \frac{\phi}{2.10^4 \cdot B_{rce}} \quad (11)$$

Using the stator area, the height of the stator wheel (h_E) is calculated, as follows (12).

$$h_e = \frac{S_{ce}}{L_{mag}} \quad (12)$$

In this way, the stator outer diameter becomes:

$$D_{ext} = D_{int} + 2 \cdot P_t + 2 \cdot h_e \quad (13)$$

The shaft diameter of the PMSG was calculated using (14), being related to the apparent power and the rated speed.

$$D_{axle} = 2,8 \cdot \sqrt[4]{\frac{S}{n}} \quad (14)$$

The air gap parameters were determined as a function of the average air gap area (S_g), calculated as:

$$S_g = \frac{b_p \cdot L_{mag} + (b' + 2 \cdot \mu_D) \cdot \frac{b_p}{\tau_c} \cdot L_{mag}}{2} \quad (15)$$

Referring to Fig.4, the addition of the stator teeth is calculated as a percentage of b' , defined as:

$$\mu_D = K_D \cdot b' \quad (16)$$

In (16) K_D is a percentage value for the base length of the teeth.

Taking the air gap area and the magnetic flux under rated conditions, the air gap flux density (B_g) is determined as:

$$B_g = \frac{\phi}{10^4 \cdot S_g} \quad (17)$$

Table VI shows the values of the length increment from 15% to 30% in relation to b' , considering the air gap average area (S_g) and air gap flux density (B_g) calculated for each of the increment.

TABLE VI
AIR-GAP FLUX DENSITY VS STATOR TEETH LENGHT

K_D	μ_D (cm)	S_g (cm ²)	B_g (G)	B_g (T)
0.150	0.178	747.83	8447	0.8447
0.175	0.208	754.88	8367	0.8367
0.200	0.238	761.92	8290	0.8290
0.225	0.268	768.97	8214	0.8214
0.250	0.297	776.01	8139	0.8139
0.275	0.327	783.06	8066	0.8066
0.300	0.357	790.10	7994	0.7994

It was found that the additional length K_D of 0.200 maintained the air gap flux density within the pre-determined values recommended by Table IV.

Based on the air gap flux density and linear current density, the air gap length (g) is calculated according to (18) [4].

$$g = 0,3 \cdot \frac{A}{10^6 \cdot B_g} \cdot \tau \quad (18)$$

Considering the rated data from Table II and the predetermined values according to Table VII, the stator design can be finished and the results were presented in the Table VIII.

TABLE VII
STATOR DESIGN PARAMETERS

Parameter	Predetermined Values [4]
Air-gap Flux Density (B_g)	0.860 T
Linear Current Density (A)	40000 A/m
Number of Slots per Pole	2
Winding Factor	0.966
D_{int}/L_{mag} (ϵ)	1.800
Maximum Current Density (σ)	5 A/mm ²
Cable Diameter (D_C)	2.90 mm
Insulation and Spacing (width) (R_L)	6.80 mm
Insulation and Spacing (depth) (R_P)	12.40 mm
Stator Teeth Additional Length (K_D)	0.20
Stator Flux Density	1.200 T

TABLE VIII
PMSG STATOR PARAMETERS

Parameter	Calculated Value
Number of Pole Pairs (p)	6
Phase Current (I_p)	3155 A
Power Factor ($\cos(\phi)$)	0.85
Number of Stator Slots (N_{CE})	72
Volumetric Factor (M)	725446.14 cm ³
Inner Diameter (D_{int})	109.30 cm
Magnetic Length (L_{mag})	60.72 cm
Number of Stator Conductors (N_{tc})	72
Linear Current Density (A)	66200 A/m
Number of Set of Cables (C_c)	80
N° Cables in Width (C_L)	10
N° Cables in Depth (C_P)	8
Tooth Opening (b')	1.19 cm
Tooth Opening on the Stator Wheel (b'')	1.23 cm
Magnetic Flux Under Rated Load Conditions (ϕ)	6316641 Mx
Outer Diameter (D_{ext})	125.09 cm
Axle Diameter (D_{axle})	20.13 cm
Air Gap Flux Density (B_g)	0.829 T
Air Gap Length (g)	0.70 cm

B. Stator Windings

In alternating current windings, more specifically in the stator, an analysis of windings symmetry and balancing is necessary. Thus, the number of generator symmetries is initially evaluated through (19) [22].

$$N_{symmetries} = GCD[N_{TC}; p] = GCD[72; 6] = 6 \quad (19)$$

The generator has 6 symmetries, each one consisting of 2 poles. Then the magnetic balancing is checked, using (20):

$$X = \frac{N_{TC}}{3 \cdot N_{symmetries}} = \frac{72}{3 \cdot (6)} = 4 \quad (20)$$

The result obtained in (20) is an integer, therefore, the generator stator winding is symmetrical and balanced, which made it possible to distribute the windings in the stator slots. For this the number of conductors per slot (N_{CS}) and the number of conductors per phase (N_{CP}) were determined, through (21) and (22), respectively.

$$N_{CS} = \frac{N_{TC}}{N_{CE}} = \frac{72}{72} = 1 \quad (21)$$

$$N_{CP} = \frac{N_{TC}}{3} = \frac{72}{3} = 24 \quad (22)$$

The total electrical degrees (D_{ET}) and slot electrical degrees (D_{ES}) allowed the distribution of winding stator and phases. In this way, the electrical degrees were calculated as:

$$D_{ET} = 2p \cdot 180^\circ = (12) \cdot (180^\circ) = 2130^\circ E \quad (23)$$

$$D_{ES} = \frac{D_{ET}}{N_{CE}} = \frac{2130^\circ E}{72} = 30^\circ E \quad (24)$$

In this step, coil pitch (Y_{coil}), the phase pitch (Y_{phase}) and the pole pitch (Y_{pole}) are calculated, thus characterising the stator windings. In (25) the phase pitch is determined.

$$Y_{phase} = \frac{120^\circ}{D_{ES}} = \frac{120^\circ E}{30^\circ E} = 4 \text{ teeth} \quad (25)$$

Therefore, the phase pitch has 4 teeth (from the first to the fifth slot). To calculate the pole pitch in number of slots (Y_{pole}) and the coil pitch (Y_{coil}), the total number of coils (N_{BT}), the number of coils per phase (N_{BF}) and the number of coils per pole and phase (N_{BPF}) are determined respectively by (26), (27) and (28).

$$N_{BT} = \frac{N_{CE}}{2} = \frac{72}{2} = 36 \quad (26)$$

$$N_{BF} = \frac{N_{BT}}{N_{phase}} = \frac{36}{3} = 12 \quad (27)$$

$$N_{BPF} = \frac{N_{BT}}{2p \cdot N_{phase}} = \frac{36}{(12) \cdot (3)} = 1 \quad (28)$$

The stator winding have 36 coils, 12 coils per phase and 1 coil per pole and phase. In this way, the pole pitch in slots, becomes:

$$Y_{pole} = \frac{N_{CE}}{N_{BF}} = \frac{72}{12} = 6 \text{ teeth} \quad (29)$$

Therefore, 6 teeth (first to seventh slot). For this particular winding, the coils are prepared considering the pitch shortened by 1 slot, i.e. the coil pitch will be:

$$Y_{coil} = Y_{pole} - 1 = 6 - 1 = 5 \text{ teeth} \quad (30)$$

Then, the coil pitch from the first to the sixth slot is performed. This analysis allowed the distribution of the stator windings, as shown in Fig. 5, where the respective connections of the coils in active poles are represented [22].

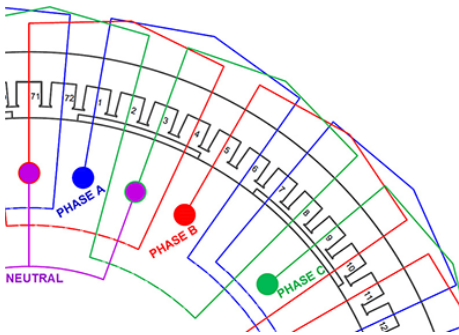


Fig. 5. Stator winding distribution-Front Diagram.

The Table IX shows the main data of the distributed three-phase winding [22].

TABLE IX
PMSG COIL PARAMETERS

Parameter	Calculated Value
Number of Conductors per Slot (N_{CS})	1
Number of Conductors per Phase (N_{CP})	24
Total Electrical Degrees (D_{ET})	2130°
Slot Electrical Degrees (D_{ES})	30°
Phase Pitch (Y_{phase})	4 teeth
Total Number of Coils (N_{BT})	36
Number of Coils per Phase (N_{BF})	12
Number of Coils per Pole and Phase (N_{BPF})	1
Pole Pitch in Number of Slots (Y_{pole})	6 teeth
Coil Pitch (Y_{coil})	5 teeth

C. Surface Mounted Permanent Magnet Rotor (SMPMR)

1) *NdFeB - SMPMR*: The SMPMR are radially magnetized and their magnets are placed on the periphery of the rotor, mechanically fixed or fixed by glue. Another important characteristic is the fact that, among the main arrangements, this one in particular makes it possible to obtain a slightly higher air gap flux density using the same volume of magnets. However, its application is limited to a speed range of the order of 3000 rpm [6].

The SMPMR design is based on the stator parameters and as first step it is calculated the ratio between the induced voltage in the generator windings at no load and the phase voltage under rated load ϵ , performed according to (31) [5].

$$\epsilon = \frac{0,5 \cdot \sqrt{2} \cdot \pi^2 \cdot D_{int}^2 \cdot L_{mag} \cdot k_a \cdot A \cdot B_g \cdot \cos(\varphi) \cdot \eta \cdot \frac{n}{60}}{P \cdot 10^6} \quad (31)$$

In (31), $\cos(\varphi)$ is the generator power factor and η is the generator efficiency.

The armature reaction factor considers the specificities of each arrangement, and in this work, the direct axis armature reaction factor (k_{fd}) and the quadrature armature factor (k_{fq}) were set at (32) and (33) respectively [5].

$$k_{fd} = \frac{1}{\pi} [\psi \cdot \pi + \text{sen}(\psi\pi) + (1 + \frac{h}{g})(\pi - \psi\pi - \text{sen}(\psi\pi))] \quad (32)$$

$$k_{fq} = \frac{1}{\pi} [(\frac{1}{1 + \frac{h}{g}})(\psi\pi - \text{sen}(\psi\pi)) + \pi(1 - \psi) + \text{sen}(\psi\pi)] \quad (33)$$

Where h is the height of the magnet slot. Using the factors defined in (32) and (33) it is observed that there are no slots for the magnets, therefore, the slot height (h) is null, hence $k_{fd} = k_{fq} = 1$. The PM utilization coefficient (ζ) can be calculated according to (34).

$$\zeta = \frac{2 \cdot P \cdot k_{sc} \cdot k_{fd} \cdot (1 + \epsilon)}{2p \cdot \pi^2 \cdot f \cdot B_r \cdot H_c \cdot h_{ma} \cdot L_{mag} \cdot \psi \cdot \tau} \quad (34)$$

In (34) k_{sc} is the overload coefficient, defined as the ratio between the overload power and the rated power of the generator, B_r is the remanence and H_c is the coercivity of the PM, since N-50 NdFeB PM being adopted. The air gap flux density as a function of PM height, remanence and air gap length can be calculated using (35) [23].

$$B_g = \frac{h_m \cdot B_r}{g + h_m} \quad (35)$$

Equation (35) was used together with (34) to allow determination of the PM utilisation coefficient, resulting in:

$$\zeta = \frac{2 \cdot 10^6 \cdot k_{sc} \cdot k_{fd} \cdot P \cdot (B_r - B_g) \cdot (1 + \epsilon)}{\pi^2 \cdot 2p \cdot g \cdot B_g \cdot \psi \cdot \tau \cdot L_{mag} \cdot f \cdot B_r \cdot H_c} \quad (36)$$

After determining ζ , the overall PM utilization coefficient (C_v) is calculated, using (37):

$$C_v = \frac{2 \cdot k_{sc} \cdot k_{fd} \cdot (1 + \epsilon)}{\pi^2 \cdot \zeta} \quad (37)$$

Thus, the total volume of PM (V_{MT}) becomes:

$$V_{MT} = C_v \cdot \frac{P_{ativa}}{f \cdot B_r \cdot H_c} \quad (38)$$

Based on the total volume, the individual volume of each PM is calculated, however, first it is necessary to determine their dimensions. The opening radius of the PM w_{ma} is the same as b_p , while the depth l_{ma} has a dimension equal to the magnetic length of the generator L_{mag} , enabling the PM height h_{ma} to be determined using (39).

$$h_{ma} = \frac{V_{MT}}{2p \cdot L_{ma} \cdot w_{ma}} \quad (39)$$

With this parameter defined, it was possible to analyse the flux densities in the regions of interest and the elaboration of a 2-D model of the generator, represented by Fig. 6.

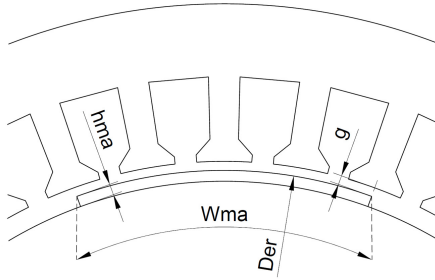


Fig. 6. Magnet and Air Gap Parameters.

2) *AlNiCo - SMPMR*: The AlNiCo SMPMR design was developed considering the same geometrical, magnetic and electrical parameters of the stator, having similar steps to the one developed in section II-A. However, due to the different magnetic characteristics of the AlNiCo PM, some changes were necessary, since the values calculated through (36) presented values out of the with recommended range between $\zeta = 0.30 - 0.81$ [5], [23], [24]. The volume of PM found without application of an adjustment, results in an undersized value, leading to a height smaller than necessary to produce the desired air gap flux density.

3) *Third Contribution*: To solve this problem, simulations were performed in order to determine a correction factor for the AlNiCo PM (k_{AlNiCo}), being this factor applied in (38), resulting in (40).

$$V_{MTa} = k_{AlNiCo} \cdot C_v \cdot \frac{P_{ativa} \cdot 10^6}{f \cdot B_r \cdot H_c} \quad (40)$$

In order to determine the value of k_{AlNiCo} , different PM heights were tested. Table X presents the results of the air

TABLE X
PM HEIGHT X NUMERICAL AIR GAP FLUX DENSITY

h_{ma} (cm)	B_{gN} (T)
2.50	0.470
4.50	0.785
4.60	0.797
4.70	0.809
4.80	0.820
4.90	0.831
5.00	0.841

gap inductions obtained B_{gN} numerically as a function of the respective heights.

The PM height that resulted in the desired flux density (h'_{ma}) was used in (41).

$$k_{AlNiCo} = \frac{2p \cdot L_{ma} \cdot w_{ma} \cdot h'_{ma} \cdot f \cdot H_c \cdot B_r}{C_v \cdot P_{ativa} \cdot 10^6} \quad (41)$$

In (41) $L_{ma} = L_{mag}$ and $w_{ma} = b_p$.

D. SPMR Parameters Results

Table XI present the data for the NdFeB and AlNiCo magnets.

TABLE XI
PM DATA

Parameter	PM Data	
	NdFeB PM	AlNiCo PM
Overload Coefficient (K_{sc})	1.15	1.15
Remanence (B_r)	1.443 T	1.060 T
Coercitivity (H_c)	983770 (A/m)	112100 (A/m)

Considering the data in Table XI and (31) to (41) the rotor parameters were calculated and the results are presented in Table XII.

TABLE XII
PMSG ROTOR PARAMETERS

Parameter	Calculated Value	
	NdFeB	AlNiCo
No-load and Rated Load Voltage Ratio (ϵ)	1.421	1.421
PM Utilisation Coefficient (ζ)	0.706	3.170
PM Overall Utilization Coefficient (C_v)	0.799	0.178
PM AlNiCo correction factor (k_{AlNiCo})	-	1.9494
PM Opening Radius (w_{ma})	18.60 cm	18.60 cm
PM Depth (l_{ma})	60.72 cm	60.72 cm
PM Height (h_{ma})	0.94 cm	2.51 cm
PM Corrected Height (h'_{ma})	-	4.90 cm

E. PMSG Flux Density Calculation Structure

The remaining magnetic parameters are the flux densities in the generator specific regions, which were used for comparison with the numerical model results. These regions of interest are the air gap, the stator, the rotor and the stator teeth.

In the rotor, the area is calculated by (42):

$$S_{cr} = \frac{(D_{er} - 2 \cdot h_{ma} - D_{axle}) \cdot L_{mag}}{4} \quad (42)$$

With the rotor area S_{cr} the rotor flux density B_{cr} was determined by (43).

$$B_{cr_a} = \frac{\phi}{10^4 \cdot S_{cr}} \quad (43)$$

In the stator teeth, an average flux density has been considered. And in this way, the average area over the single pole of the teeth S_D can be determined according to (44).

$$S_D = \frac{b'(1 + 2 \cdot \mu_D) + b''}{2} \cdot L_{mag} \cdot \frac{b_p}{\tau_c} \quad (44)$$

ince the average area is determined in (44), it is possible to obtain the teeth flux density B_D according to (45).

$$B_D = \frac{\phi}{10^4 \cdot S_D} \quad (45)$$

Tables XIII present the flux densities for the NdFeB PM and AlNiCo PM [4].

TABLE XIII
PMSG FLUX DENSITY - ANALYTICAL METHOD

Area of Interest	Calculated (T)	Recommended (T)
Air Gap	0.829	0.820 - 0.900
Stator	1.200	1.000 - 1.200
Rotor PM NdFeB	0.240	≤0.700- 1.200
Rotor PM AlNiCo	0.240	≤0.700- 1.200
Stator Teeth	1.842	1.600 - 1.800

III. 2-D NUMERICAL RESOLUTION

A. Magnetostatic Formulation

The numerical resolution model obeys Maxwell's laws and pre-established boundary conditions. The magnetostatic problem formulation uses the vectors B , A , J and the magnetic permeability of the material $\mu_{(B)}$ that varies as function of B . The relationship among these vectors can be seen in the equation (46):

$$-\frac{1}{\mu_{(B)}} \nabla^2 \vec{A} = \vec{J} \quad (46)$$

In (46), \vec{J} is the current vector density, \vec{A} is the magnetic vector potential and \vec{B} is the vector flux density. The current sources were imposed in the armature windings with the value of magnetomotive force.

B. 2-D Numerical Resolution - NdFeB PM and AlNiCo PM

Based on the PMSG dimensions obtained through the analytical model, a 2-D simulation was performed in a magnetostatic regime in order to numerically obtain the values of the inductions in each part of the PMSG and then compare the results with those obtained analytically, allowing the validation [10].

During the 2-D model preparation, the materials were assigned to each region of the PMSG and the size of the mesh discretization was investigated. The materials used for the simulation were 1020 steel in the stator and rotor, 304 stainless steel in the generator shaft and N-50 NdFeB PM and LNGT-72 9 AlNiCo PM in the rotor.

Fig. 7a illustrates the flux density colour map across the machine geometry for the NdFeB PM and respectively, in Fig. 7b, for the AlNiCo PM is illustrated. These maps allow us to analyse the saturation levels in the regions of the PMSG.

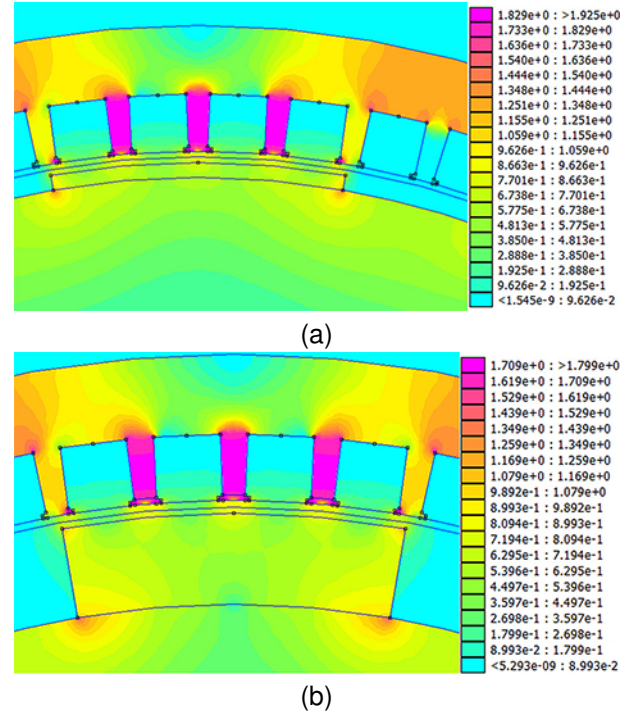


Fig. 7. 2-D Colour Map Static Simulation.

To capture the air gap flux density in the stator, rotor and stator tooth more accurately, an explorer line, illustrated in red, is used, as shown in Fig. 8

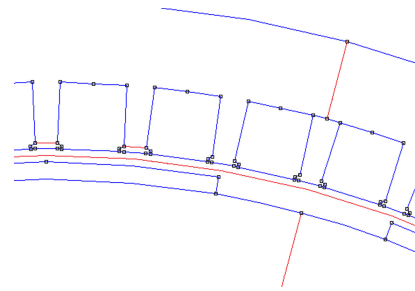


Fig. 8. Explorer Line.

The flux densities obtained by the numerical method, for the two types of PM were entered in Table XIV.

TABLE XIV
PMSG FLUX DENSITY - 2-D NUMERICAL METHOD

Area of Interest	NdFeB (T)	AlNiCo (T)
Air Gap	0.834	0.831
Stator	1.230	1.151
Rotor	0.257	0.244
Stator Tooth	1.789	1.681

The use of the explorer line in the air gap allowed the flux density waveform to be captured, for both arrangements, as

Fig. 9a and Fig. 9b correspondingly.

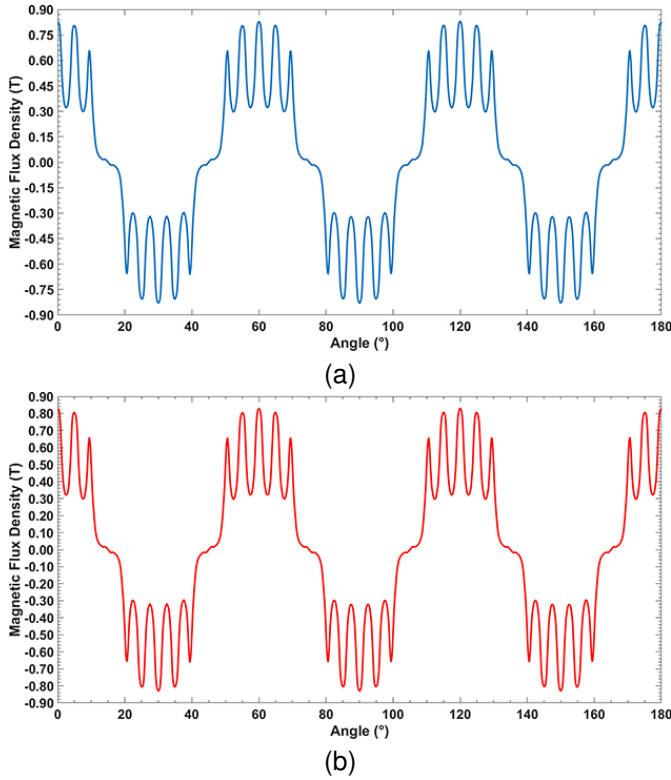


Fig. 9. Air Gap Flux Density Waveform.

IV. IMPACT OF STATOR SLOTS IN THE AIR GAP FLUX DENSITY WAVEFORM

The air gap waveform obtained in the PMSG not only depend on the distribution of the stator windings, geometry and type of PM used, but also on the number of slots of the stator. In order to determine this effect, the frequency due to the slots was analysed for both PM arrangements and compared to the harmonic spectrum.

The angular frequency of the stator currents (ω) is used to calculate the resulting angular frequency of the rotating field in the air gap (ω_{cg}), which is related to the number of poles, according to (47) [22].

$$\omega_{cg} = \frac{\omega}{p} \quad (47)$$

Therefore, the frequency of the rotating field (f_{cg}) in Hz can be calculated by:

$$f_{cg} = \frac{\omega_{cg}}{2\pi} \quad (48)$$

With the calculated field frequency, the harmonic frequency due to the slots (f_r) is determined, as (49).

$$f_r = \left(\frac{2 \cdot N_{CE}}{2p} + 1 \right) \cdot f_{cg} \quad (49)$$

Table XV shows the values of the frequencies for the study of harmonics.

TABLE XV
AIR GAP FREQUENCIES

Parameter	Calculated Value
Angular Frequency of the Stator Currents	911.06 rad/s
Angular Frequency of the Rotating Field in the Air Gap	151.84 rad/s
Frequency of the Rotating Field in the Air Gap	24.17 Hz
Harmonic Frequency Due to Slots	314.17 Hz

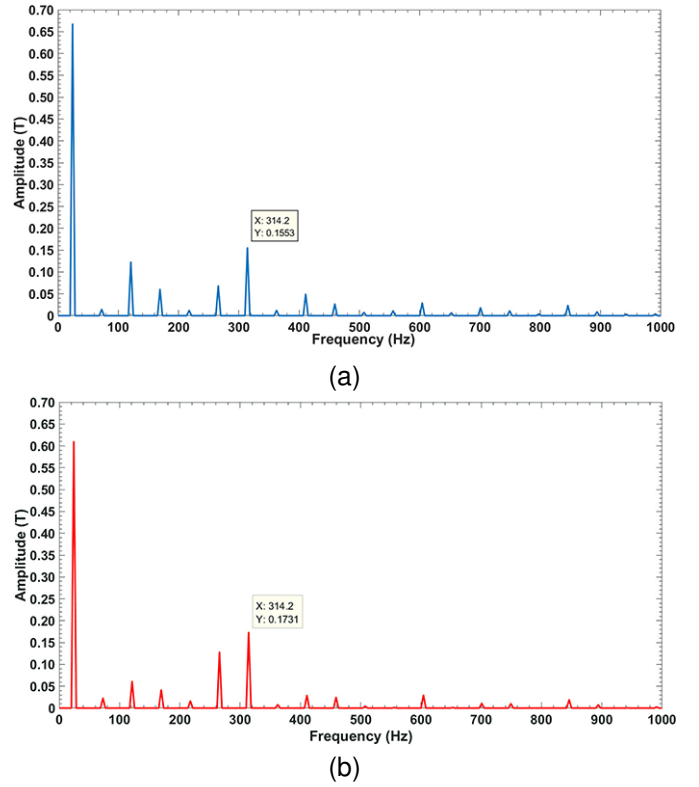


Fig. 10. Harmonic Analysis.

The spectra of Fig.10a and Fig.10b represent the air gap flux density harmonics, obtained for the two PM configurations (N-50 NdFeB and 9 AlNiCo) respectively. In the figures the thirteenth harmonic is highlighted, being this one corresponding to f_r , in both PM arrangements. Comparing the two spectra, we notice a small increase in the amplitude of the thirteenth harmonic observed in Fig. 10b in relation to the level obtained in the spectrum of Fig. 10a.

TABLE XVI
HARMONIC AMPLITUDE

Harmonic Order	NdFeB (T)	AlNiCo (T)
Fundamental	0.662	0.609
Third	0.014	0.023
Fifth	0.123	0.061
Seventh	0.060	0.041
Ninth	0.011	0.016
Eleventh	0.068	0.128
Thirteenth	0.155	0.173

Regarding other harmonic frequencies, it was found that for the NdFeB PM the fundamental, fifth and seventh have higher amplitudes compared to the AlNiCo PM, according to Table

XVI. Only the third and ninth have higher amplitudes for the AlNiCo PM.

V. ANALYSIS OF THE INFLUENCE OF 2-D FEM MESHES

In order to evaluate the impact of the mesh density, simulations were performed considering different mesh sizes and their impact on the peak value of the air gap flux density (B_{gmax}) and the impact on the average of ten highest values of air gap flux density (B_{gmed}). This analysis also allowed to determine the convergence point for the obtained magnetic flux density values.

A. Analysis of Material Mesh Size in the Air Gap Induction

In Table XVII mesh size values were assigned for the PMSG materials, whereby in this first analysis the mesh size of the air gap was kept fixed with 1 mm size and the external environment with 10 mm size as well as for the rotor shaft. The stator, rotor and PM materials were simulated with different mesh sizes. The air gap flux density was evaluated with 50,000 points.

TABLE XVII
GENERATOR MATERIAL MESH SIZE ANALYSIS

PMSG Mesh Size	$B_{gmax}(T)$	$\Delta_{max}(T)$	$B_{gmed}(T)$	$\Delta_{med}(T)$
10	0.8337	0.0000	0.8334	0.0000
9	0.8337	0.0000	0.8334	0.0000
8	0.8337	0.0000	0.8334	0.0000
7	0.8337	0.0000	0.8334	0.0000
6	0.8337	0.0000	0.8334	0.0000
5	0.8337	0.0000	0.8334	0.0000
4	0.8336	0.0001	0.8333	0.0001
3	0.8335	0.0001	0.8332	0.0001
2	0.8336	0.0001	0.8334	0.0002
1	0.8338	0.0002	0.8337	0.0003

In Table XVII the air gap flux density does not show large variation with mesh sizes greater than 4, indicating that for smaller values, the air gap flux density tends to converge to a value greater than 0.8337 T, however, regardless of the mesh size, the variation is negligible, that is, about 0.17 mT between the extreme values for the maximum value and 0.26 mT for the average value.

B. Analysis of Air Gap Mesh Size in the Air Gap Induction

In this second analysis, the mesh size assigned to the materials was kept with a fixed size at 10 for the outer and shaft, 5 for the slots and PM, 3 for the rotor and stator, whereas, the mesh size of the air gap was evaluated for different sizes starting from 4.00 to 0.50 mm. In Table XVIII the data of peak value of air gap flux density for different mesh sizes captured with 50,000 sample points were arranged.

TABLE XVIII
AIR GAP MESH SIZE ANALYSIS

Air Gap Mesh Size	B_{gmax}	Δ_{max}	B_{gmed}	Δ_{med}
4.00	0.8329	0.0000	0.8328	0.0000
3.00	0.8329	0.0000	0.8328	0.0000
2.00	0.8348	0.0018	0.8346	0.0018
1.00	0.8337	0.0011	0.8334	0.0012
0.75	0.8341	0.0005	0.8339	0.0005
0.50	0.8340	0.0001	0.8338	0.0001

Referring Table XVIII as the air gap mesh size approaches the air gap width, there is a sharp increase in flux density, indicating that mesh values exceeding the width of the air gap, leads to inaccuracies. However, using sufficiently small mesh values, it is observed that the values of air gap flux density, show little variation, about 0.0001 T for the largest value and for the average value. The Fig. 11a and 11b illustrates different mesh sizes for the Air gap, according to the data in Table XVIII.

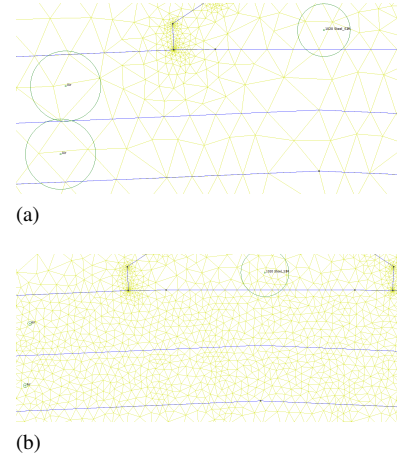


Fig. 11. Variation of Air Gap Mesh Size.

VI. 3-D NUMERICAL RESOLUTION

A. Magnetotransient Formulation

The formulation of the problem in magnetotransient regime becomes (50).

$$\nabla \times v \nabla \times \vec{A} = \vec{J} - \sigma \left(\frac{\partial \vec{A}}{\partial t} \right) - \sigma \nabla V + \nabla \times \vec{H}_c + \sigma v \times \nabla \times \vec{A} \quad (50)$$

In (50) the constants v and σ are the magnetic reluctivity and the electrical conductivity, respectively. In (50), V is electric scalar potential of the source, \vec{H}_c is the coercive field strength, when there are permanent magnets in the geometry, the vector \vec{J} is the current density of the stator conductors and \vec{A} is the magnetic potential vector. Fig. 12 illustrates the boundary conditions of the problem.

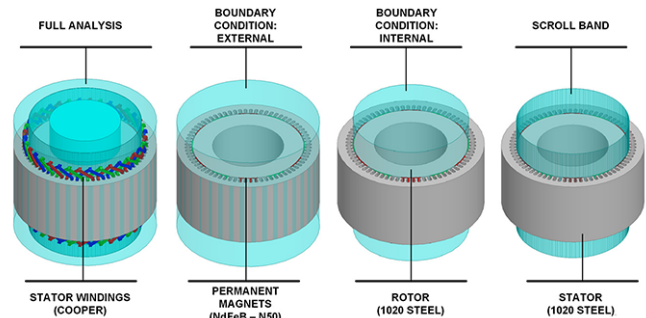


Fig. 12. Boundary Conditions and Materials Used.

Fig. 13a and Fig. 13b represent the colour maps of the inductions obtained in the magnetotransient simulations for both

PM arrangements. The values obtained by the 3-D numerical method were also used for comparison with the developed analytical model. In the Table XIX the values obtained by the 3-D method for the flux densities in the regions of interest were disposed.

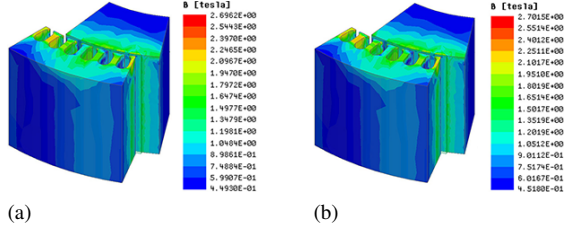


Fig. 13. 3-D Colour Map Dynamic Simulation.

TABLE XIX
PMSG FLUX DENSITY - 3-D NUMERICAL METHOD

Area of Interest	NdFeB (T)	AlNiCo (T)
Stator	1.04 - 1.19	1.05 - 1.20
Rotor	0.29 - 0.44	0.29 - 0.45
Stator Tooth	1.79 - 1.94	1.80 - 1.95

Unlike the 2-D FEM simulation in the magnetostatic regime, the 3-D FEM simulation is performed in the magnetotransient regime and made it possible, in addition to the flux densities in the regions of interest, to extract quantities such as the electric voltage and current produced by the PMSG [14]. The voltages and currents waveforms obtained can be seen in Fig.14 and Fig.15 respectively.

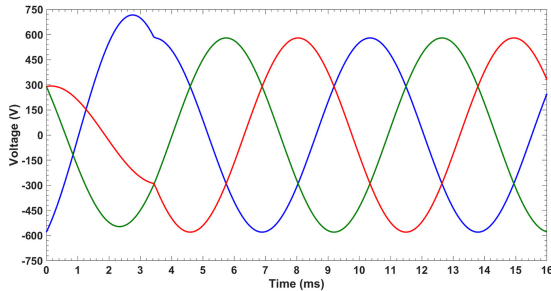


Fig. 14. PMSG Three-phase Voltage

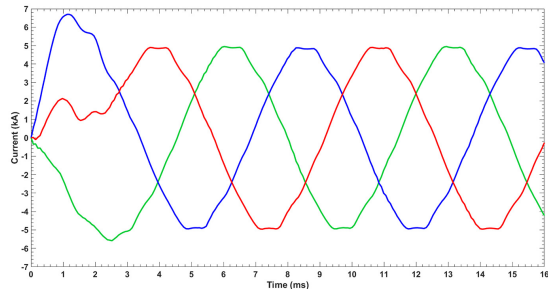


Fig. 15. PMSG Three-phase Current

The voltage and current values are shown in Table XX.

TABLE XX
3-D NUMERICAL METHOD - RESULTS

Parameter	Numerical Result
Peak Phase Voltage	579.70 V
Phase Voltage (V_{p3d})	409.90 V
Line Voltage (V_{l3d})	709.90 V
Peak Current	4.86 kA
Current (I_{p3d})	3.44 kA

VII. RESULTS ANALYSIS

The validation of the developed analytical model was done by comparing the values obtained by the analytical model with the values obtained by the 2-D, 3-D numerical model.

A. 2-D Numerical Model - Flux Density Analysis

The flux densities in the areas of interest for both PM (NdFeB and AlNiCo) with the same rotor configuration were confronted. Table XXI presents the comparative data for the rotor with NdFeB N-50 PM and AlNiCo 9 LNGT 72 PM.

TABLE XXI
RESULTS - ANALYTICAL AND 2-D NUMERICAL

Region	NdFeB			
	Recommended (T)	Analytical (T)	FEM (T)	Error (%)
Air Gap	0.820-0.900	0.8290	0.8341	0.61
Stator	1.000-1.200	1.2000	1.2301	2.51
Rotor	≤0.700-1.200	0.2404	0.2569	6.86
Stator Tooth	1.600-1.800	1.8424	1.7889	2.90
Region	AlNiCo			
	Recommended (T)	Analytical (T)	FEM (T)	Error (%)
Air Gap	0.820-0.900	0.8290	0.8306	0.19
Stator	1.000-1.200	1.2000	1.1511	4.07
Rotor	≤0.700-1.200	0.2404	0.2440	1.50
Stator Tooth	1.600-1.800	1.8424	1.6812	8.75

It is noted from Table XXI that the results obtained by the analytical and numerical 2-D FEM model for NdFeB PM have relative error of 0.61% for the air gap, 2.51% for the stator core, 6.86% for the rotor core and 2.90% for the stator tooth. The relative errors between the models for the areas of interest obtained by the 2-D FEM model for the AlNiCo 9 LNGT 72 PM were low, about 0.19% for the air gap, 4.07% for the stator, 1.50% for the rotor and 8.75% for the teeth.

B. 3-D Numerical Model - Flux Density Analysis

The comparison between the analytical model and the 3-D FEM numerical model was performed in the same way as the 2-D FEM simulation. In Table XXII it is observed the values obtained by the models and their respective absolute errors.

VIII. DISCUSSION

NdFeB magnets are considered rare earth PM and have a higher cost per mass than AlNiCo PM. The proposal of the work aims to create an option for the use of NdFeB or AlNiCo PM. For that to be the method used in NdFeB PM must be modified, because the remanence and coercivity values are different.

TABLE XXII
RESULTS - ANALYTICAL AND 3-D NUMERICAL

Region	NdFeB			ΔB (mT)
	Recommended (T)	Analytical (T)	Numerical (T)	
Stator	1.000-1.200	1.2000	1.1900	10.0
Rotor	≤ 0.700 -1.200	0.2404	0.2900	49.6
Stator Tooth	1.600-1.800	1.8424	1.7900	52.4
Region	AlNiCo			ΔB (mT)
	Recommended (T)	Analytical (T)	Numerical (T)	
Stator	1.000-1.200	1.2000	1.2000	0.0
Rotor	≤ 0.700 -1.200	0.2404	0.2900	49.6
Stator Tooth	1.600-1.800	1.8424	1.8000	42.4

IX. CONCLUSION

The analytical methodology developed in this work was able to determine the electrical, magnetic and geometric parameters of a PMSG, for NdFeB PM and AlNiCo PM, and the results were supported through computational simulations in numerical software resolution by the FEM applied to magnetic problems. Comparing the analytical method applied to the NdFeB PM with the 2-D numerical method there was an average relative error of 3.22%, and the relative error obtained for the air gap was calculated as 0.61%. When the PM material was AlNiCo type, the correction applied to the PM volume in the analytical method allowed the PMSG rotor design with this material. By comparing the methods, the average relative error was calculated at 3.62% and for the air gap the relative error was calculated at 0.19%. The 3-D numerical method compared to the developed analytical method applied to the NdFeB PM, presented average absolute error of 37 mT.

These results indicate that the developed analytical method presented is effective and the results obtained are satisfactory and indicated that the electrical and magnetic parameters determined analytically have relative errors less than 10%.

In this work the main contributions were the readjustment of the speed and frequency table specifically for a 145 Hz machine. Another contribution was the development of a parameter that considers the extension of the tip of the stator teeth, considering that this dimension influences the values of air gap flux density. Finally the readjustment of the method used for NdFeB PM particularly for AlNiCo PM, as an option of cheaper PM.

REFERENCES

- [1] I. Al-Bahadly, *Wind Turbines*. Rijeka: IntechOpen, 2011.
- [2] S. Nanda and M. Sengupta, "Design, fabrication and analytical investigations on a permanent magnet synchronous generator," in *2014 IEEE International Conference on Power Electronics, Drives and Energy Systems (PEDES)*, pp. 1–4, 2014.
- [3] J. A. Güemes, A. M. Iraolagoitia, P. Fernández, and M. P. Donsión, "Comparative study of pmsm with integer-slot and fractional-slot windings," in *The XIX International Conference on Electrical Machines - ICEM 2010*, pp. 1–6, 2010.
- [4] A. Martignoni, *Alternating Current Machinery*. Porto Alegre: Globo, 7 ed., 2008.
- [5] J. F. Gieras, *Permanent magnet motor technology : design and applications*. Polônia: CRC Press, 2010.
- [6] R. Krishnan, *Permanent Magnet Synchronous and Brushless DC Motor Drives*. Estados Unidos da América: CRC Press, Setembro, 2010.
- [7] S. Teymoori, A. Rahideh, H. Moayed-Jahromi, and M. Mardaneh, "2-d analytical magnetic field prediction for consequent-pole permanent magnet synchronous machines," *IEEE Transactions on Magnetics*, vol. 52, no. 6, pp. 1–14, 2016.

- [8] D. Carpenter, S. Deleanu, C. Nguyen, M. Lau, and M. M. Rahman, "A study on determination of parameters for permanent magnet synchronous machine by comparing load tests and finite element analysis," in *2011 24th Canadian Conference on Electrical and Computer Engineering (CCECE)*, pp. 000587–000592, 2011.
- [9] M. Ozeki and S. Shimomura, "Comparative study of integrated radial-axial flux rotor motor using ferrite magnet," in *2017 20th International Conference on Electrical Machines and Systems (ICEMS)*, pp. 1–6, 2017.
- [10] O. Côté, A. Chebak, and J.-F. Méthot, "Design and optimization of a high torque in-wheel surface-mounted pm synchronous motor using concentrated winding," in *2013 International Electric Machines & Drives Conference*, pp. 863–870, 2013.
- [11] A. Vijay and N. P. Kumar, "Effect of demagnetization fault in spmsm using finite element analysis," in *2021 IEEE 2nd International Conference on Smart Technologies for Power, Energy and Control (STPEC)*, pp. 1–6, 2021.
- [12] A. J. Sorgdrager and A. J. Grobler, "Influence of magnet size and rotor topology on the air-gap flux density of a radial flux pmsm," in *2013 IEEE International Conference on Industrial Technology (ICIT)*, pp. 337–343, 2013.
- [13] Q. He and X. Bao, "Reducing cogging torque in permanent-magnet synchronous motors by auxiliary teeth method," in *2016 IEEE 11th Conference on Industrial Electronics and Applications (ICIEA)*, pp. 1488–1495, 2016.
- [14] A. A. Diriyé, Y. Amara, and G. Barakat, "Three-dimensional modeling of permanent magnets synchronous machines using a 3d reluctance network," in *2018 XIII International Conference on Electrical Machines (ICEM)*, pp. 2304–2310, 2018.
- [15] P. Naveen, P. K. N. K. Sriganesh, T. Rajesh, and K. Sushmitha, "Stator fault analysis of permanent magnet synchronous motor using finite element method," in *2019 4th International Conference on Recent Trends on Electronics, Information, Communication & Technology (RTEICT)*, pp. 655–660, 2019.
- [16] J. Faiz, Z. Valipour, M. Shokri-Kojouri, and M. A. Khan, "Design of a radial flux permanent magnet wind generator with low coercive force magnets," in *2016 2nd International Conference on Intelligent Energy and Power Systems (IEPS)*, pp. 1–7, 2016.
- [17] H. Y. Lv, X. Y. Wang, J. J. Du, and L. H. Zhu, "Analytical calculation of pmsg optimization for compact er-eps application," in *2015 IEEE International Conference on Applied Superconductivity and Electromagnetic Devices (ASEMD)*, pp. 551–552, 2015.
- [18] L. Dang, N. Bernard, N. Bracikowski, and G. Berthiau, "Analytical model and reluctance network for high-speed pmsm design optimization application to electric vehicles," in *2016 XXII International Conference on Electrical Machines (ICEM)*, pp. 1359–1365, 2016.
- [19] Z. Guo and L. Chang, "Fem study on permanent magnet synchronous generators for small wind turbines," pp. 641–644, 2005.
- [20] C.-Y. Hsiao, S.-N. Yeh, and J.-C. Hwang, "Design of high performance permanent-magnet synchronous wind generators," *Energies*, pp. 7105–7124, 2014.
- [21] Vestas Wind Systems A/S, *General Specification V112–3.0 MW 50/60 Hz*. Dinamarca, 2010. Documento N°.: 0011-9181 V03.
- [22] P. Bimbra, *Electrical Machinery*, pp. 816–865. Khanna Publishers, 2020.
- [23] G. Slemon and X. Liu, "Core losses in permanent magnet motors," *IEEE Transactions on Magnetics*, vol. 26, no. 5, pp. 1653–1655, 1990.
- [24] G. Todorov and B. Stoev, "Analytical model for sizing the magnets of permanent magnet synchronous machines," 10 2015.



Ademir Pelizari is an electrical engineer graduated from the University of Mogi das Cruzes (UMC), São Paulo, Brazil in 2002. He completed his master's and doctoral degrees in 2009 and 2015, respectively. He currently works as an Adjunct Professor at the Federal University of ABC (UFABC) in the areas of electromechanical devices and electrical machines.



Alfeu Joãozinho Sguarezi Filho is Adjunct Professor at the Federal University of ABC (UFABC) with Doctor's degrees in Electrical Engineering from the Faculty of Electrical and Computer Engineering of the State University of Campinas (Unicamp) in 2007 and 2010, respectively. He is a Senior Member of the IEEE and researcher and author of several articles in national and international scientific journals and book chapters in the areas of electrical machines, machine control, power electronics, wind energy.



Gabriel Rodrigues Bruzinga is an electrical engineer graduated from the federal university of ABC (2018) and is currently in the postgraduate program with a master's degree in electrical engineering. The focus of the project involves the design of permanent magnet synchronous generators (PMSG) with a focus on wind energy.



Igor Oliani holds a Bachelor's degree in Science and Technology from the Federal University of ABC (2019) where he is currently pursuing a degree in Energy Engineering and participating in the Master's program in Electrical Engineering. His research line is focused on electrical systems and power electronics applied to electric motor drives and electric vehicles.